Elastic response of monolayer $Si_{1-x}Ge_x$

Xiaoyang Ma,[1] Tong Yang,[2] Dechun Li,[1,*] and Yuanping Feng[3,†]

[1]*School of Information Science and Engineering, Shandong University, 72 Binhai Road, Qingdao 266237, China*

[2]*Department of Applied Physics, The Hong Kong Polytechnic University, Hung Hom, Hong Kong SAR, China*

[3]*Department of Physics, National University of Singapore, 2 Science Drive 3, Singapore 117551 and Centre for Advanced 2D Materials, National University of Singapore, 6 Science Drive 2, Singapore 117546*

(Received 16 February 2022; revised 10 July 2022; accepted 21 July 2022; published 29 July 2022)

The elastic response of monolayer silicon-germanium alloys ($Si_{1-x}Ge_x$, $0 \leqslant x \leqslant 1$) is investigated using first-principles calculations. It is found that the atomic arrangement of monolayer $Si_{1-x}Ge_x$ alloys has a significant impact on their elastic anisotropy, which can be categorized by their crystal systems. The hexagonal $Si_{1-x}Ge_x$ is elastically isotropic because of high symmetry, while some rectangular and oblique $Si_{1-x}Ge_x$ are elastically anisotropic because of the presence of the zigzag interface. The degree of anisotropy is related to the width and ratio of silicene/germanene strips in the $Si_{1-x}Ge_x$ superlattice structure. This work provides a guideline for experimentally realizing this series of materials that may find applications in $Si_{1-x}Ge_x$-based optoelectronics and flexible electronics.

DOI: 10.1103/PhysRevB.106.024114

I. INTRODUCTION

Over the past two decades, the research of ultrathin two-dimensional (2D) nanomaterials has reached an unprecedented level owing to their unique chemical or physical features [1–6]. Benefiting from the high surface-volume ratio and quantum confinement effect, 2D materials have been substantiated to possess extraordinary electric, optical, catalytic, and other properties [7–10]. For example, graphene can sustain extremely high in-plane mechanical strains, current densities, and thermal conductivity [11]. Excellent electronic properties have also been found successively for other 2D materials such as phosphorene with various phases [12–14]. Along with the expansion of the family of 2D materials and a growing understanding of their exotic fundamental properties, various potential applications have been proposed [15–19]; e.g., the lattice-confined materials stimulate a rising area of "confinement catalysis with 2D materials" due to the intriguing confinement environments for active sites [9]. In addition to the striking electronic properties and catalytic applications, mechanical properties, including high in-plane stiffness and extremely low flexural rigidity, which are significantly different from those in bulk materials [20–22], are also induced in the 2D forms. The high modulus of elasticity makes 2D materials attractive in strain sensors, fibers, protective coatings, etc. [23–26]. The elastic responses upon different loading (also called isotropy/anisotropy) make some 2D materials promising in optoelectronics and flexible electronics applications [27–30]. Since mechanical strain can greatly modify the electronic, optical, and thermal properties [22,31], it plays an important role in the applications of nanomaterials [32,33]. Therefore, there must be more investigations of mechanical properties as well as elastic responses, especially studying how these properties vary with the crystal structure (particularly the microstructure) and the chemical composition of materials [34,35].

As silicon (Si) and germanium (Ge) are the cornerstones of the current electronic industry, to better integrate the nanomaterials into current devices, systems containing Si or Ge, especially silicon germanium ($Si_{1-x}Ge_x$), which could combine both the superior properties of germanene and the synthesis advantages of silicene, have been arousing tremendous interest [36–38]. With Ge doped, $Si_{1-x}Ge_x$ alloy has been reported to possess a larger thermoelectric figure of merit [39], higher carrier mobility [40,41], and less reactivity [42] than silicene. The nanoscale and functionalized $Si_{1-x}Ge_x$ are predicted to be promising materials for nanoelectronics and nano-optoelectronics [43–45]. The high-quality $Si_{1-x}Ge_x$ growth with precise control of composition x and layer thickness has been reported [46,47]. According to the previous studies, single crystal SiGe layers can be fabricated by several techniques, such as molecular beam epitaxy [48], layer exchange technique [49,50], and ion implantation method [51–53]. Even though monolayer $Si_{1-x}Ge_x$ has not been synthesized so far, the recent reported quasi-free-standing silicene [54] and germanene [55] make their synthesis possible in the near future since $Si_{1-x}Ge_x$ can be formed by adding dopants into the silicene/germanene monolayer, which can be realized using the ion implantation strategy.

Since synthesis strategies such as selective ion implantation may induce anisotropy in the nanocrystals, and the isotropy/anisotropy plays an important role in diverse applications such as dislocation and transformations [56–59], the investigations of elastic responses for $Si_{1-x}Ge_x$, especially elastic isotropy/anisotropy, is necessary and valuable in the fabrication of Si-based/Ge-based nanodevices. In the

*dechun@sdu.edu.cn

†phyfyp@nus.edu.sg

past few years, 2D $Si_{1-x}Ge_x$ has been proved to be energetically stable due to similar covalent radii, and their electronic, optoelectronic, magnetic, and thermal dynamic properties have been explored abundantly from the theoretical point of view [50–52]. However, to the best of our knowledge, the mechanical properties of $Si_{1-x}Ge_x$, especially the elastic responses upon the loading in different directions, have not been fully investigated. Thus, in this paper, we performed first-principles calculations to investigate the elastic response of monolayer $Si_{1-x}Ge_x$ and aimed to identify factors that may affect their isotropy/anisotropy from the theoretical perspective. Our calculations predict three crystal systems for the monolayer $Si_{1-x}Ge_x$ with different isotropic/anisotropic properties. Among them, the hexagonal $Si_{1-x}Ge_x$ exhibit elastic isotropy, similar to silicene, germanene, and siligene [60–62], whereas the rectangular and oblique $Si_{1-x}Ge_x$ are elastically anisotropic, which is found to be closely related to the presence of the zigzag silicene/germanene interface. Moreover, the degree of elastic anisotropy could be associated with the width of zigzag silicene/germanene nanoribbons.

II. COMPUTATIONAL DETAILS

For 2D systems, the generalized Hooke's law can be written as

$$\begin{bmatrix}\sigma_{xx}\\ \sigma_{yy}\\ \sigma_{xy}\end{bmatrix} = \begin{bmatrix}C_{11} & C_{12} & C_{16}\\ C_{12} & C_{22} & C_{26}\\ C_{16} & C_{26} & C_{66}\end{bmatrix}\begin{bmatrix}\varepsilon_{xx}\\ \varepsilon_{yy}\\ 2\varepsilon_{xy}\end{bmatrix} = \begin{bmatrix}S_{11} & S_{12} & S_{16}\\ S_{12} & S_{22} & S_{26}\\ S_{16} & S_{26} & S_{66}\end{bmatrix}^{-1}\begin{bmatrix}\varepsilon_{xx}\\ \varepsilon_{yy}\\ 2\varepsilon_{xy}\end{bmatrix}, \quad (1)$$

where σ_{ij} $(i, j = x, y)$ is the stress tensor on the face perpendicular to $k_i (i = x, y)$ in the direction $k_j (j = x, y)$, C_{ij} $(i, j = 1, 2,$ or $6)$ is the stiffness constant, $S_{ij} (i, j = 1, 2,$ or $6)$ is the compliance constant, and ε_{ij} $(i, j = x, y)$ is the strain; note that $2\varepsilon_{xy} = 2\varepsilon_{yx} = \varepsilon_6$. According to the definitions of Young's moduli and the Poisson ratio, the mechanical properties of 2D materials including Young's moduli (in-plane stiffness), Poisson ratios, and shear modulus can be calculated from the compliance constants [63],

$$\begin{aligned} Y_x &= \frac{1}{S_{11}},\\ Y_y &= \frac{1}{S_{22}},\\ \upsilon_{xy} &= -S_{12}Y_x,\\ \upsilon_{yx} &= -S_{12}Y_y. \end{aligned} \quad (2)$$

To investigate the mechanical properties along an arbitrary direction, we rotate the axis (x, y) to (x', y') at an arbitrary angle θ; then the elastic compliance constants at an arbitrary angle θ are given as follows:

$$\begin{aligned} S'_{11} &= S_{11}\cos^4\theta + (2S_{12} + S_{66})\cos^2\theta\sin^2\theta + S_{22}\sin^4\theta,\\ S'_{22} &= S_{11}\sin^4\theta + (2S_{12} + S_{66})\cos^2\theta\sin^2\theta + S_{22}\cos^4\theta,\\ S'_{12} &= (S_{11} + S_{22} - S_{66})\cos^2\theta\sin^2\theta + S_{12}(\cos^4\theta + \sin^4\theta),\\ S'_{66} &= 4(S_{11} + S_{22} - 2S_{12})\cos^2\theta\sin^2\theta + S_{66}(\cos^2\theta - \sin^2\theta)^2,\\ S'_{16} &= (2S_{11} - 2S_{12} - S_{66})\sin\theta\cos^3\theta\\ &\quad + (2S_{12} - 2S_{22} + S_{66})\sin^3\theta\cos\theta,\\ S'_{26} &= (2S_{11} - 2S_{12} - S_{66})\sin^3\theta\cos\theta\\ &\quad + (2S_{12} - 2S_{22} + S_{66})\sin\theta\cos^3\theta \end{aligned} \quad (3)$$

Obviously, for a 2D system, both compliance tensor S_{ij} and the stiffness tensor C_{ij} are functions of orientation. Subjected to the uniform displacement boundary condition, the averaged stress and strain can be described in terms of the shear modulus G and so-called area modulus K [56,64],

$$\begin{aligned} \langle\sigma_{ij}\rangle &= 2K^V\varepsilon_p^0\delta_{ij} + 2G^V e_{ij}^0 \ (i, j = 1, 2),\\ \langle\varepsilon_{ij}\rangle &= \frac{1}{2K^R}\sigma_p^0\delta_{ij} + \frac{1}{2G^R}s_{ij}^0 \ (i, j = 1, 2), \end{aligned} \quad (4)$$

where V and R represent the Voigt and Reuss averages [65], respectively. δ_{ij} is the Kronecker delta function. $s_{ij}(e_{ij})$ is the deviatoric stress (strain) $s_{ij} = \sigma_{ij} - \sigma_p\delta_{ij}$ $(e_{ij} = \varepsilon_{ij} - \varepsilon_p\delta_{ij})$. $\sigma_p = (\sigma_{11} + \sigma_{22})/2$ and $\varepsilon_p = (\varepsilon_{11} + \varepsilon_{22})/2$ are the area stress and averaged strain, respectively. The elastic anisotropy index A^{SU} which is a universal measure to quantify the degree of anisotropy of crystal [56,64] can be expressed as

$$A^{\mathrm{SU}} = \sqrt{\left(\frac{K^V}{K^R} - 1\right)^2 + 2\left(\frac{G^V}{G^R} - 1\right)^2}. \quad (5)$$

The 2D structure is predicted via the cluster expansion (CE) method as implemented in the Alloy Theoretic Automated Toolkit (ATAT) [66]. In the CE scheme, given the lattice information of parent structures and their related symmetry operations, the supercell lattice frames can be constructed [67]. Then, according to the atomic arrangement in lattice frames and symmetries, monolayer $Si_{1-x}Ge_x$ is generated. Density functional theory (DFT) calculations were carried out to investigate the elastic response of 2D $Si_{1-x}Ge_x$ using the Vienna *ab initio* simulation package (VASP) [68]. The projector augmented wave (PAW) method and the Perdew-Burke-Ernzerhof form of generalized gradient approximation (GGA PBE) [68,69] were adopted to describe the core-electron interaction and the exchange-correlation interaction, respectively. A plane-wave basis with cutoff energy of 600 eV was used to expand the electronic wave function. The convergence criterion for the total energy and the geometric optimization was set to 1×10^{-6} eV and 0.01 eV/ Å, respectively. k-point meshes of $15 \times 15 \times 1$ have been utilized. Additionally, a vacuum layer of 30 Å has been inserted to alleviate the spurious interlayer interaction in the out of plane direction.

III. RESULTS AND DISCUSSION

Before discussing the elastic response of 2D $Si_{1-x}Ge_x$ alloys, we first evaluate their synthesis feasibility.

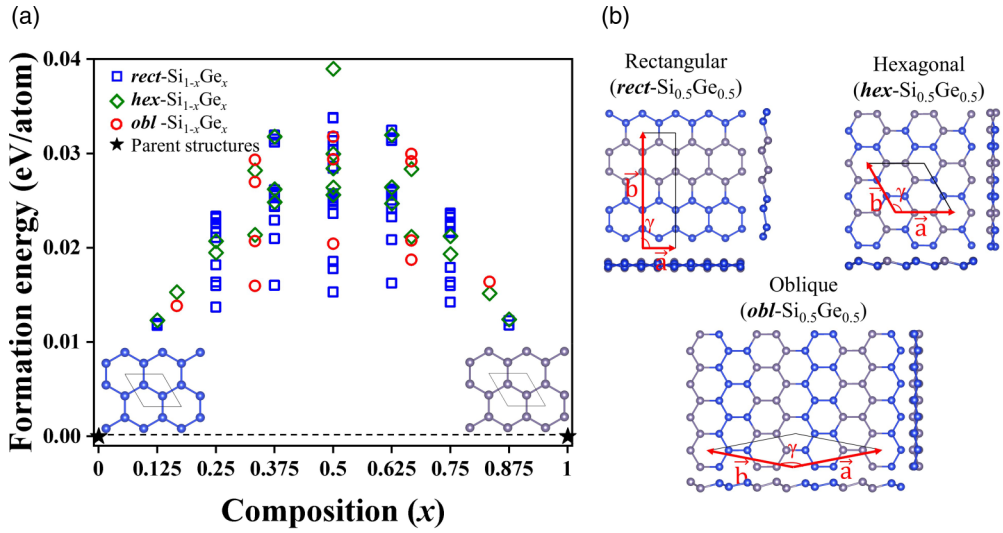

FIG. 1. Formation energies and different crystal systems of monolayer $Si_{1-x}Ge_x$. (a) Formation energy of 105 monolayer $Si_{1-x}Ge_x$ supercell structures containing up to eight atoms. The blue squares, green diamonds, and red circles represent 2D rectangular (*rect*-), hexagonal (*hex*-), and oblique (*obl*-) lattices, respectively. The black stars connected by the dashed line are the parent structures (silicene and germanene). (b) The lowest-energy structures of *rect*-, *hex*- and *obl*-$Si_{1-x}Ge_x$ at $x = 0.5$ among the 105 monolayer $Si_{1-x}Ge_x$ supercell structures containing up to eight atoms.

Considering the similar low buckled honeycomb structures, monolayer silicene and germanene are used as parent structures (Fig. S1 in the Supplemental Material (SM) [70]). All the possible monolayer $Si_{1-x}Ge_x$ supercell structures containing up to eight atoms are generated in CE simulation using the algorithm developed by Hart and Forcade [71]. The energy-composition (x) diagram of 2D $Si_{1-x}Ge_x$ is presented in Fig. 1(a). The formation energies are obtained by $E_f(x) = E_{Si_{1-x}Ge_x} - xE_{Ge} - (1-x)E_{Si}$, where $E_{Si_{1-x}Ge_x}$, E_{Ge}, and E_{Si} are the total energy per atom of $Si_{1-x}Ge_x$, germanene, and silicene, respectively. It is clear that the formation energies of all configurations in the whole composition range are positive and vary from 10 to 38 meV/atom, suggesting the endothermic process of forming binary $Si_{1-x}Ge_x$. Nevertheless, the formation energies are small enough that nanoscale $Si_{1-x}Ge_x$ could be fabricated fairly easily, as demonstrated in recent experiments [36,44,72].

According to the rotational symmetry, monolayer $Si_{1-x}Ge_x$ in Fig. 1(a) can be classified into three crystal systems, i.e., 2D rectangular (*rect*-), hexagonal (*hex*-), and oblique (*obl*-) crystals, represented by blue squares, green diamonds, and red circles, respectively. Generally, the *rect*-$Si_{1-x}Ge_x$ is energetically favored over *hex*- and *obl*-$Si_{1-x}Ge_x$. The minimum energy structures of $Si_{1-x}Ge_x$ ($x = 0.25$, 0.5, and 0.75) displayed in Fig. S2 [70] prefer phase segregation. The stability induced by the symmetric arrangement of atoms has also been found in three-dimensional (3D) materials such as alkali-doped calcium silicate hydrate [73]. This result can be explained by the intrinsic phase-separated state of crystals with two symmetry-distinct phases, and it is consistent with the phase diagram in which monolayer $Si_{1-x}Ge_x$ shows the presence of the two-phase region at low temperature across the entire range [74]. Besides, the lowest-energy $Si_{1-x}Ge_x$ ($x = 0.5$) with different crystal systems shown in Fig. 1(b) suggests that the phase segregation state is not related to the crystal system. With the same crystal system, $Si_{1-x}Ge_x$ consisting of a zigzag silicene/germanene interface is energetically more stable because of the smaller lattice mismatch between silicene and germanene in the zigzag direction (4.91% of 3.87 Å for silicene or 4.68% of 4.06 Å for germanene) than that in other directions. As specified in Table S1 [70], the *rect*-$Si_{0.5}Ge_{0.5}$ consisting of a zigzag silicene/germanene interface is energetically favored compared to *rect*-$Si_{0.5}Ge_{0.5}$ consisting of an armchair silicene/germanene interface. The lattice mismatch leads to a small tensile/compressive strain which in turn results in the change of bond length R and buckling height Δ.

To explore how the mechanical properties evolve with the tensile/compressive strain, calculations are carried out to investigate the elastic property of monolayer $Si_{1-x}Ge_x$. By applying the infinitesimal strain ε from -0.015 to 0.015 and with an increment of 0.005, the elastic stiffness tensor C_{ij}, which is also related to the second-order elastic constants, can be derived from the energy-strain curves based on the changes of the strain energy: $E = \frac{1}{2}\sum_{i,j=1}^{6} C_{ij}\varepsilon_{ij}\varepsilon_{ji}$ [75]. The calculated mechanical properties including in-plane stiffness, Poisson ratios, and elastic anisotropy index of the minimum energy structures *obl*-, *rect*-, and *hex*-$Si_{0.5}Ge_{0.5}$ are shown in Table S2 [70]. Based on the calculated elastic constants, the mechanical stability is confirmed via Born stability criteria [76] (see Sec. 4 in the SM [70]). It is noted that subject to small in-plane deformation, silicene and germanene are suggested to have an isotropic Young's modulus (Y) and Poisson ratio (v) [60,61]. Therefore, monolayer $Si_{1-x}Ge_x$ is expected to be mechanically isotropic as well. However, the slight deviation from a perfect circle in polar diagrams of *rect*- and *obl*-$Si_{0.5}Ge_{0.5}$ (Fig. 2) show that the in-plane stiffness and Poisson ratio have weak anisotropy, while for *hex*-$Si_{0.5}Ge_{0.5}$ the nearly perfect circles represent the isotropic properties.

The anisotropy/isotropy can be quantified by the universal anisotropy index A^{SU}. When a crystal is isotropic,

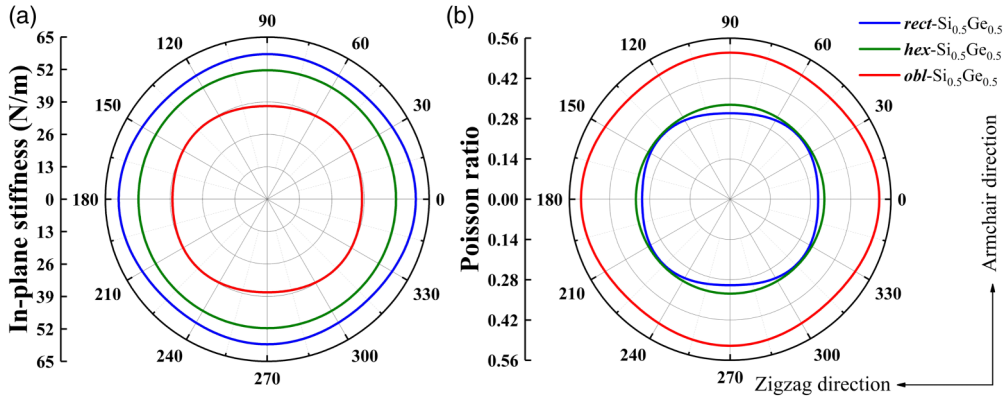

FIG. 2. Polar diagram of the (a) in-plane stiffness and (b) Poisson ratios for the minimum energy $Si_{1-x}Ge_x$ at $x = 0.5$ with different crystal systems. The blue, olive, and red lines represent the *rect*-, *hex*-, and *obl*-$Si_{0.5}Ge_{0.5}$, respectively.

$\frac{G^V}{G^R} = 1$, $\frac{K^V}{K^R} = 1$, and thus $A^{\mathrm{SU}} = 0$. According to Eq. (5), the elastic anisotropy diagram (EAD) of $Si_{1-x}Ge_x$ is constructed in the $(\frac{G^V}{G^R}, \frac{K^V}{K^R})$ space as shown in Fig. 3. It can be found that *hex*-$Si_{1-x}Ge_x$ is at the point $(\frac{G^V}{G^R} = 1, \frac{K^V}{K^R} = 1)$, which indicates the elastic isotropy. This is predictable since the average area/shear moduli are simplified to $K^V = K^R = (C_{11} + C_{12})/2$, $G^V = G^R = (C_{11} - C_{12})/2$. The points for *obl*- and *rect*-$Si_{1-x}Ge_x$ are scattered but the majority are within $A^{\mathrm{SU}} \leqslant 0.003$, implying the weak anisotropy of $Si_{1-x}Ge_x$. This can be explained by the similarity of silicon and germanium atoms. The distribution of A^{SU} for $Si_{1-x}Ge_x$ is in agreement with the EAD for 2D crystals [64].

Unlike 2D *hex*-crystals, which are known to be strongly correlated with elastic isotropy, the elastic isotropy/anisotropy for *rect*- and *obl*-crystals is closely associated with atomic arrangements. This is consistent with the scattered blue squares and red circles in Fig. 3. Even though most of the structures have weak anisotropy ($A^{\mathrm{SU}} \leqslant 0.003$), there is one exception,

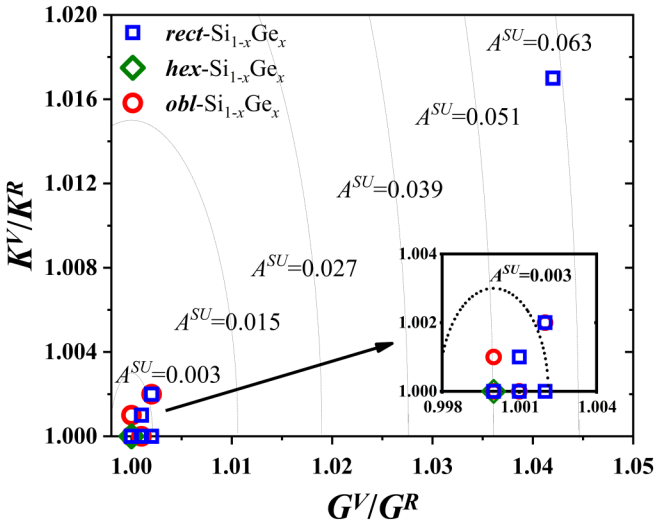

FIG. 3. Elastic anisotropy diagram for $Si_{1-x}Ge_x$. The blue squares, green diamonds, and red circles represent *rect*-, *hex*-, and *obl*-$Si_{1-x}Ge_x$ with different compositions, respectively. The contour lines (A^{SU}) are obtained from Eq. (5). The inset in the figure shows the scatters around $G^V/G^R = 1$.

$A^{\mathrm{SU}} = 0.062$. The corresponding *rect*-$Si_{1-x}Ge_x$ possesses a relatively strong anisotropy and the structure is shown in Fig. 4(a). This structure is composed of alternating zigzag Si and Ge atomic chains, and there exist some small changes in bond lengths (a few percent) but significant changes in bond angles. As to buckling height (see Table S3 [70]), the value between two Si atoms decreases from 0.447 Å in silicene to 0.007 Å, while that between two Ge atoms increases from 0.675 Å in germanene to 0.917 Å in this *rect*-SiGe. The dramatic decrease of buckling height between two Si atoms leads to a tensile strain in the silicene strip, whereas the increase between two Ge atoms results in the compressive strain in the germanene strip. As reported by Mortazavi *et al.*, for both silicene and germanene, this strain effect is particularly pronounced at higher loading conditions, especially along the zigzag direction [77]. Hence, due to the high internal strain loading induced by lattice mismatch, this structure is expected to show anisotropic mechanical properties. The in-plane stiffnesses are 60.773 and 47.161 N/m, and the Poisson ratios are 0.234 and 0.182 along the zigzag direction and armchair direction, respectively. This is in sharp contrast to the reported isotropic 2D siligene (see Table S4 [70]). The lower in-plane stiffness in the armchair direction indicates the higher fracture strength, making this *rect*-SiGe more flexible to deform but harder to break in this direction.

Compared to the structure in Fig. 4, the buckling heights for both Si and Ge atoms (0.477 and 0.684 Å, respectively) of *rect*-SiGe consisting of armchair silicene/germanene strips only increased slightly due to the small compressive loading (see Table S1 [70]). Since the buckling parameter is irrespective of the direction under a small strain [77], this structure exhibits isotropy as shown in Fig. S3 [70]. In-plane stiffness is 51.294 N/m, and the Poisson ratio is 0.334. In order to further understand the reason for isotropy/anisotropy in monolayer $Si_{1-x}Ge_x$, we investigated the atomic arrangements of *rect*- and *obl*-$Si_{1-x}Ge_x$ and found that all structures with $A^{\mathrm{SU}} \neq 0$ comprise zigzag silicene/germanene strips. As shown in Fig. S4 [70], the minimum energy $Si_{1-x}Ge_x$ ($x = 0.25$, 0.5, and 0.75) structures consisting of zigzag silicene/germanene strips exhibit weak anisotropy rather than isotropy. Similar to *rect*-SiGe in Fig. 4, the anisotropy can be explained by the internal strains which are deeply involved in the silicene/germanene interface (see Table S5 [70]). That is,

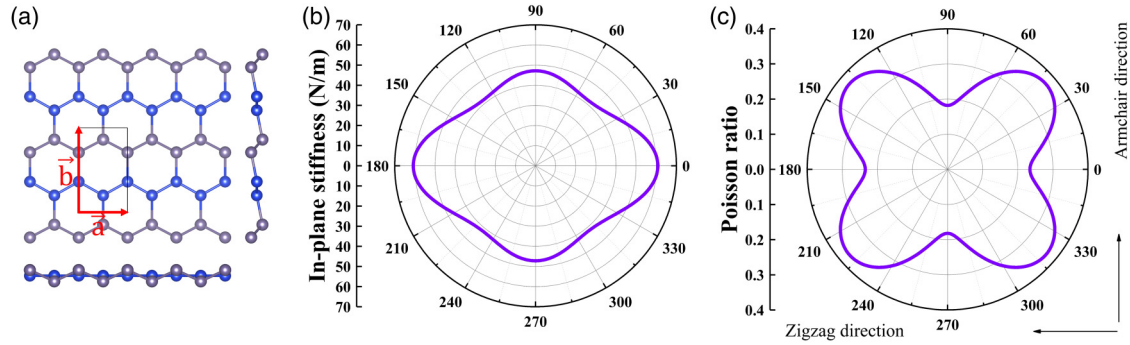

FIG. 4. Structure and mechanical properties of monolayer *rect*-SiGe consisting of zigzag silicene nanoribbon (width of 1) and zigzag germanene nanoribbon (width of 1). (a) The top and side views of the structure. (b), (c) Polar diagram of the in-plane stiffness and Poisson ratios.

wider silicene or germanene strips will restrain the opposite internal strains, resulting in the weak anisotropy of monolayer $Si_{1-x}Ge_x$. Thus, we can say that the elastic anisotropy degree A^{SU} of the monolayer $Si_{1-x}Ge_x$ could be influenced by the width of silicene or germanene strips, similar to the thermoelectric figure of merit in silicon-germanium superlattice nanowires, which depends on the periodic length [78]. This elastic anisotropy affected by the zigzag edge state may resemble those of the silicene/germanene superlattice [78] but would be significantly modified due to the interface effect similar to the thermal properties [79,80].

To investigate the correlation between the degree of anisotropy and zigzag silicene/germanene interface as well as compositions, the elastic isotropy/anisotropy of 105 $Si_{1-x}Ge_x$ is evaluated. Even though most structures are essentially isotropic, along with the increase of Ge composition, some *rect*- and *obl*-$Si_{1-x}Ge_x$ show a small degree of deviation from $A^{SU} = 0$, especially a blue square located at $x = 0.5$ which corresponds to the structure in Fig. 4(a) possessing a relatively strong anisotropy. Besides, by estimating the possibility of $A^{SU} \neq 0$ at each composition (the inset in Fig. 5), we found that monolayer $Si_{1-x}Ge_x$ is most likely to be anisotropic at the intermediate composition ~0.5. This is reasonable as more zigzag silicene/germanene interfaces can be found when the composition of Si is approximately equal to that of Ge. Therefore, it is deduced that the isotropy/anisotropy of *rect*- and *obl*-$Si_{1-x}Ge_x$ is very likely attributed to the zigzag silicene/germanene interface as well as compositions. As monolayer $Si_{1-x}Ge_x$ with pair coupling has been proved to possess the Dirac cone [74,81], by modulating the zigzag interface, isotropic or anisotropic Dirac cone materials could be generated. In addition, considering the anisotropy of 2D square crystals is more relevant to the atomic arrangements similar to the rectangular and oblique crystals [64], we can predict that the square $Si_{1-x}Ge_x$ containing the zigzag silicene/germanene interface would be elastically anisotropic.

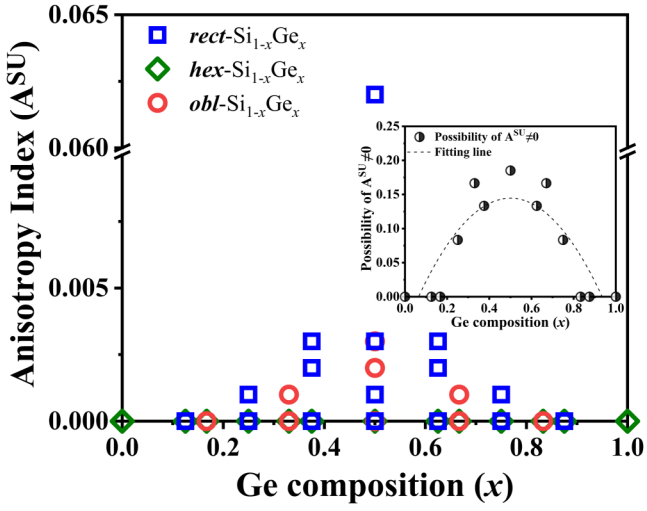

FIG. 5. Elastic anisotropy-composition diagram for $Si_{1-x}Ge_x$. The fitting line in the inset picture represents the anisotropy possibility at each x. The possibility p is calculated via $p = n(x)_{A^{SU}\neq 0}/n(x)$, where $n(x)_{A^{SU}\neq 0}$ is the number of $Si_{1-x}Ge_x$ with $A^{SU} \neq 0$ at the composition x, $n(x)$ is the total number of $Si_{1-x}Ge_x$ at composition x.

IV. CONCLUSION

In conclusion, the elastic anisotropy diagram is obtained for monolayer $Si_{1-x}Ge_x$ that are grouped into three systems (rectangular, hexagonal, and oblique crystals) using 2D elastic anisotropy index A^{SU}. The similarity of silicon and germanium causes a little range of anisotropy index ($A^{SU} < 0.063$) for monolayer $Si_{1-x}Ge_x$. Moreover, the *hex*-$Si_{1-x}Ge_x$ is elastically isotropic due to its crystal system, while for *rect*- and *obl*-$Si_{1-x}Ge_x$, the elastic isotropy and anisotropy are mainly related to the zigzag silicene/germanene interface as well as compositions (or periodic length). The monolayer $Si_{1-x}Ge_x$ is most likely to be anisotropic at the intermediate composition $x \sim 0.5$, and the anisotropy is mostly contributed to the opposite strain loading in the zigzag silicene/germanene interface. Thus, unlike the usual way that the degree of isotropy/anisotropy is tuned by modulating interactions such as hydrogen bonding, halogen bonding, and $\pi \cdots \pi$ interactions, in the present study, it is found that isotropy/anisotropy can be affected by the atomic arrangement. The understanding of intermolecular interaction makes it possible to precisely control the elastic isotropy/anisotropy during synthesis and is of fundamental importance for property-oriented crystal design. Furthermore, this study lays the foundation for the applications of 2D $Si_{1-x}Ge_x$ with respect to the elastic response.

ACKNOWLEDGMENTS

This research is supported by the China Postdoctoral Science Foundation Grant No. 2021M702002 and the Postdoctoral Applied Research Project of Qingdao. The authors acknowledge the Centre for Advanced 2D Materials, the National University of Singapore, and the National Supercomputing Centre of Singapore for providing computational resources.

[1] A. A. Balandin, S. Ghosh, W. Bao, I. Calizo, D. Teweldebrhan, F. Miao, and C. N. Lau, Superior thermal conductivity of single-layer graphene, Nano Lett. **8**, 902 (2008).

[2] S. Balendhran, S. Walia, H. Nili, S. Sriram, and M. Bhaskaran, Elemental analogues of graphene: Silicene, germanene, stanene, and phosphorene, Small **11**, 640 (2015).

[3] K. S. Novoselov, A. K. Geim, S. V. Morozov, D. Jiang, Y. Zhang, S. V. Dubonos, I. V. Grigorieva, and A. A. Firsov, Electric field effect in atomically thin carbon films, Science **306**, 666 (2004).

[4] Z. Ni, Q. Liu, K. Tang, J. Zheng, J. Zhou, R. Qin, Z. Gao, D. Yu, and J. Lu, Tunable bandgap in silicene and germanene, Nano Lett. **12**, 113 (2011).

[5] L. Huang, Y.-F. Zhang, Y.-Y. Zhang, W. Xu, Y. Que, E. Li, J.-B. Pan, Y.-L. Wang, Y. Liu, and S.-X. Du, Sequence of silicon monolayer structures grown on a Ru surface: From a herringbone structure to silicene, Nano Lett. **17**, 1161 (2017).

[6] H. Zhang, Ultrathin two-dimensional nanomaterials, ACS Nano **9**, 9451 (2015).

[7] P. Tao, S. Yao, F. Liu, B. Wang, F. Huang, and M. Wang, Recent advances in exfoliation techniques of layered and non-layered materials for energy conversion and storage, J. Mater. Chem. A **7**, 23512 (2019).

[8] Q. Wang, K. Xu, Z. Wang, F. Wang, Y. Huang, M. Safdar, X. Zhan, F. Wang, Z. Cheng, and J. He, van der Waals epitaxial ultrathin two-dimensional nonlayered semiconductor for highly efficient flexible optoelectronic devices, Nano Lett. **15**, 1183 (2015).

[9] L. Tang, X. Meng, D. Deng, and X. Bao, Confinement catalysis with 2D materials for energy conversion, Adv. Mater. **31**, 1901996 (2019).

[10] M. Luo, Y. Yang, Y. Sun, Y. Qin, C. Li, Y. Li, M. Li, S. Zhang, D. Su, and S. Guo, Ultrathin two-dimensional metallic nanocrystals for renewable energy electrocatalysis, Mater. Today **23**, 45 (2019).

[11] A. K. Geim, Graphene: Status and prospects, Science **324**, 1530 (2009).

[12] A. Gupta, T. Sakthivel, and S. Seal, Recent development in 2D materials beyond graphene, Prog. Mater Sci. **73**, 44 (2015).

[13] H. Jin, S. Xin, C. Chuang, W. Li, H. Wang, J. Zhu, H. Xie, T. Zhang, Y. Wan, Z. Qi, W. Yan, Y.-R. Lu, T.-S. Chan, X. Wu, J. B. Goodenough, H. Ji, and X. Duan, Black phosphorus composites with engineered interfaces for high-rate high-capacity lithium storage, Science **370**, 192 (2020).

[14] K. Novoselov, A. Mishchenko, A. Carvalho, and A. C. Neto, 2D materials and van der Waals heterostructures, Science **353**, aac9439 (2016).

[15] C. Lee, X. Wei, J. W. Kysar, and J. Hone, Measurement of the elastic properties and intrinsic strength of monolayer graphene, Science **321**, 385 (2008).

[16] S. Cahangirov, M. Topsakal, E. Aktürk, H. Şahin, and S. Ciraci, Two- and One-Dimensional Honeycomb Structures of Silicon and Germanium, Phys. Rev. Lett. **102**, 236804 (2009).

[17] L. Li, Y. Yu, G. J. Ye, Q. Ge, X. Ou, H. Wu, D. Feng, X. H. Chen, and Y. Zhang, Black phosphorus field-effect transistors, Nat. Nanotechnol. **9**, 372 (2014).

[18] M. Chhowalla, D. Jena, and H. Zhang, Two-dimensional semiconductors for transistors, Nat. Rev. Mater. **1**, 16052 (2016).

[19] J. R. Schaibley, H. Yu, G. Clark, P. Rivera, J. S. Ross, K. L. Seyler, W. Yao, and X. Xu, Valleytronics in 2D materials, Nat. Rev. Mater. **1**, 16055 (2016).

[20] M. H. Rahman, E. H. Chowdhury, D. A. Redwan, and S. Hong, Computational characterization of thermal and mechanical properties of single and bilayer germanene nanoribbon, Comput. Mater. Sci. **190**, 110272 (2021).

[21] M. G. Ahangari, A. Salmankhani, A. H. Imani, N. Shahab, and A. H. Mashhadzadeh, Density functional theory study on the mechanical properties and interlayer interactions of multi-layer graphene: Carbonic, silicon-carbide and silicene graphene-like structures, Silicon **11**, 1235 (2019).

[22] D. Akinwande, C. J. Brennan, J. S. Bunch, P. Egberts, J. R. Felts, H. Gao, R. Huang, J.-S. Kim, T. Li, and Y. Li, A review on mechanics and mechanical properties of 2D materials—graphene and beyond, Extreme Mech. Lett. **13**, 42 (2017).

[23] A. P. A. Raju, A. Lewis, B. Derby, R. J. Young, I. A. Kinloch, R. Zan, and K. S. Novoselov, Wide-area strain sensors based upon graphene-polymer composite coatings probed by Raman spectroscopy, Adv. Funct. Mater. **24**, 2865 (2014).

[24] E. Cha, M. D. Patel, J. Park, J. Hwang, V. Prasad, K. Cho, and W. Choi, 2D MoS_2 as an efficient protective layer for lithium metal anodes in high-performance Li–S batteries, Nat. Nanotechnol. **13**, 337 (2018).

[25] W. Liu, M. Liu, X. Liu, X. Wang, H.-X. Deng, M. Lei, Z. Wei, and Z. Wei, Recent advances of 2D materials in nonlinear photonics and fiber lasers, Adv. Opt. Mater. **8**, 1901631 (2020).

[26] A. Lipatov, H. Lu, M. Alhabeb, B. Anasori, A. Gruverman, Y. Gogotsi, and A. Sinitskii, Elastic properties of 2D $Ti_3C_2T_x$; Mxene monolayers and bilayers, Sci. Adv. **4**, eaat0491 (2018).

[27] Y. Niu, R. Frisenda, E. Flores, J. R. Ares, W. Jiao, D. Perez de Lara, C. Sánchez, R. Wang, I. J. Ferrer, and A. Castellanos-Gomez, Polarization-sensitive and broadband photodetection based on a mixed-dimensionality TiS_3/Si *p–n* junction, Adv. Opt. Mater. **6**, 1800351 (2018).

[28] H. Yuan, X. Liu, F. Afshinmanesh, W. Li, G. Xu, J. Sun, B. Lian, A. G. Curto, G. Ye, Y. Hikita, Z. Shen, S.-C. Zhang, X. Chen, M. Brongersma, H. Y. Hwang, and Y. Cui, Polarization-sensitive broadband photodetector using a black phosphorus vertical *p–n* junction, Nat. Nanotechnol. **10**, 707 (2015).

[29] Q. Peng, K. Hu, B. Sa, J. Zhou, B. Wu, X. Hou, and Z. Sun, Unexpected elastic isotropy in a black phosphorene/TiC_2 van der Waals heterostructure with flexible Li-ion battery anode applications, Nano Res. **10**, 3136 (2017).

[30] J. Zhao, D. Ma, C. Wang, Z. Guo, B. Zhang, J. Li, G. Nie, N. Xie, and H. Zhang, Recent advances in anisotropic two-dimensional materials and device applications, Nano Res. **14**, 897 (2021).

[31] Q. Wei and X. Peng, Superior mechanical flexibility of phosphorene and few-layer black phosphorus, Appl. Phys. Lett. **104**, 251915 (2014).

[32] K. S. Kumar, H. Van Swygenhoven, and S. Suresh, Mechanical behavior of nanocrystalline metals and alloys, Acta Mater. **51**, 5743 (2003).

[33] M. A. Meyers, A. Mishra, and D. J. Benson, Mechanical properties of nanocrystalline materials, Prog. Mater Sci. **51**, 427 (2006).

[34] C. Androulidakis, K. Zhang, M. Robertson, and S. Tawfick, Tailoring the mechanical properties of 2D materials and heterostructures, 2D Mater. **5**, 032005 (2018).

[35] Z. Li, S. Zhao, R. O. Ritchie, and M. A. Meyers, Mechanical properties of high-entropy alloys with emphasis on face-centered cubic alloys, Prog. Mater. Sci. **102**, 296 (2019).

[36] T. Bentrcia, F. Djeffal, H. Ferhati, and Z. Dibi, A comparative study on scaling capabilities of Si and SiGe nanoscale double gate tunneling FETs, Silicon **12**, 945 (2020).

[37] Z. Yu, X. Zhang, H. Zhang, Y. Huang, Y. Li, X. Zhang, and Z. Gan, Improved power conversion efficiency in radial junction thin film solar cells based on amorphous silicon germanium alloys, J. Alloys Compd. **803**, 260 (2019).

[38] J. Zhou, C. Zhang, Q. Liu, J. You, X. Zheng, X. A. Cheng, and T. Jiang, Controllable all-optical modulation speed in hybrid silicon-germanium devices utilizing the electromagnetically induced transparency effect, Nanophotonics **9**, 2797 (2020).

[39] S. Uchida, M. Lee, C.-H. Lee, and Y. Suzuki, High-temperature monolithic SiGe thermoelectric device directly heated by catalytic combustion, Appl. Phys. Lett. **120**, 053901 (2022).

[40] X. Mi, T. M. Hazard, C. Payette, K. Wang, D. M. Zajac, J. V. Cady, and J. R. Petta, Magnetotransport studies of mobility limiting mechanisms in undoped Si/SiGe heterostructures, Phys. Rev. B **92**, 035304 (2015).

[41] M. L. Lee, E. A. Fitzgerald, M. T. Bulsara, M. T. Currie, and A. Lochtefeld, Strained Si, SiGe, and Ge channels for high-mobility metal-oxide-semiconductor field-effect transistors, J. Appl. Phys. **97**, 011101 (2005).

[42] N. Kennedy, R. Duffy, G. Mirabelli, L. Eaton, N. Petkov, J. D. Holmes, C. Hatem, L. Walsh, and B. Long, Monolayer doping of silicon-germanium alloys: A balancing act between phosphorus incorporation and strain relaxation, J. Appl. Phys. **126**, 025103 (2019).

[43] N. Patel, A. Ramesha, and S. Mahapatra, Drive current boosting of *n*-type tunnel FET with strained SiGe layer at source, Microelectron. J. **39**, 1671 (2008).

[44] S. P. Rout and P. Dutta, Impact of high mobility III-V compound material of a short channel thin-film SiGe double gate junctionless MOSFET as a source, Eng. Rep. **2**, e12086 (2020).

[45] K. W. Lee and C. E. Lee, Strain-induced topological phase transition with inversion of the in-plane electric polarization in tiny-gap semiconductor SiGe monolayer, Sci. Rep. **10**, 11300 (2020).

[46] H. I. T. Hauge, S. Conesa-Boj, M. A. Verheijen, S. Koelling, and E. P. A. M. Bakkers, Single-crystalline hexagonal silicon–germanium, Nano Lett. **17**, 85 (2017).

[47] A. Bhat, O. Elleuch, X. Cui, Y. Guan, S. A. Scott, T. F. Kuech, and M. G. Lagally, High-Ge-content SiGe alloy single crystals using the nanomembrane platform, ACS Appl. Mater. Interfaces **12**, 20859 (2020).

[48] M. Sharma, M. K. Sanyal, M. K. Mukhopadhyay, M. K. Bera, B. Saha, and P. Chakraborty, Structural and morphological characterization of molecular beam epitaxy grown Si/Ge multilayer using x-ray scattering techniques, J. Appl. Phys. **110**, 102204 (2011).

[49] M. Tsuji, K. Kusano, T. Suemasu, and K. Toko, Zn-induced layer exchange of *p*- and *n*-type nanocrystalline SiGe layers for flexible thermoelectrics, Appl. Phys. Lett. **116**, 182105 (2020).

[50] K. Kusano, A. Yamamoto, M. Nakata, T. Suemasu, and K. Toko, Thermoelectric inorganic SiGe film synthesized on flexible plastic substrate, ACS Appl. Energy Mater. **1**, 5280 (2018).

[51] K. Sawano, S. Koh, Y. Shiraki, Y. Ozawa, T. Hattori, J. Yamanaka, K. Suzuki, K. Arimoto, K. Nakagawa, and N. Usami, Fabrication of high-quality strain-relaxed thin SiGe layers on ion-implanted Si substrates, Appl. Phys. Lett. **85**, 2514 (2004).

[52] T. Tabata, J. Aubin, K. Huet, and F. Mazzamuto, Segregation and activation of Ga in high Se content SiGe by UV melt laser anneal, J. Appl. Phys. **125**, 215702 (2019).

[53] K. Kim, D. C. Kang, Y. Jeong, J. Kim, S. Lee, J. Y. Kwak, J. Park, G. W. Hwang, K.-S. Lee, B.-K. Ju, J. K. Park, and I. Kim, Ion beam-assisted solid phase epitaxy of SiGe and its application for analog memristors, J. Alloys Compd. **884**, 161086 (2021).

[54] Z. Ben Jabra, M. Abel, F. Fabbri, J.-N. Aqua, M. Koudia, A. Michon, P. Castrucci, A. Ronda, H. Vach, M. De Crescenzi, and I. Berbezier, van der Waals heteroepitaxy of air-stable quasi-free-standing silicene layers on CVD epitaxial graphene/6H-SiC, ACS Nano **16**, 5920 (2022).

[55] M. Ge, M. Zong, D. Xu, Z. Chen, J. Yang, H. Yao, C. Wei, Y. Chen, H. Lin, and J. Shi, Freestanding germanene nanosheets for rapid degradation and photothermal conversion, Mater. Today Nano **15**, 100119 (2021).

[56] S. I. Ranganathan and M. Ostoja-Starzewski, Universal Elastic Anisotropy Index, Phys. Rev. Lett. **101**, 055504 (2008).

[57] M. Chicoine, S. Roorda, L. Cliche, and R. A. Masut, Directional effects during ion implantation: Lateral mass transport and anisotropic growth, Phys. Rev. B **56**, 1551 (1997).

[58] M. Meixner, E. Schöll, M. Schmidbauer, H. Raidt, and R. Köhler, Formation of island chains in SiGe/Si heteroepitaxy by elastic anisotropy, Phys. Rev. B **64**, 245307 (2001).

[59] Y. Hoshi, K. Sawano, A. Yamada, S. Nagakura, N. Usami, K. Arimoto, K. Nakagawa, and Y. Shiraki, Line width dependence of anisotropic strain state in SiGe films induced by selective ion implantation, Appl. Phys. Express **4**, 095701 (2011).

[60] C. Yang, Z. Yu, P. Lu, Y. Liu, H. Ye, and T. Gao, Phonon instability and ideal strength of silicene under tension, Comput. Mater. Sci. **95**, 420 (2014).

[61] R. Qin, C.-H. Wang, W. Zhu, and Y. Zhang, First-principles calculations of mechanical and electronic properties of silicene under strain, AIP Adv. **2**, 022159 (2012).

[62] V. Sharma, H. L. Kagdada, P. K. Jha, P. Śpiewak, and K. J. Kurzydłowski, Halogenation of SiGe monolayers: Robust changes in electronic and thermal transport, Phys. Chem. Chem. Phys. **21**, 19488 (2019).

[63] V. V. Vasiliev and E. V. Morozov, Mechanics of a composite layer, in *Advanced Mechanics of Composite Materials and Structures*, 4th ed., edited by V. V. Vasiliev and E. V. Morozov (Elsevier, Amsterdam, 2018), Chap. 2, pp. 75–189.

[64] R. Li, Q. Shao, E. Gao, and Z. Liu, Elastic anisotropy measure for two-dimensional crystals, Extreme Mech. Lett. **34**, 100615 (2020).

[65] C. M. Kube, Elastic anisotropy of crystals, AIP Adv. **6**, 095209 (2016).

[66] A. Van De Walle, M. Asta, and G. Ceder, The alloy theoretic automated toolkit: A user guide, CALPHAD: Comput. Coupling Phase Diagrams Thermochem. **26**, 539 (2002).

[67] Q. Wu, B. He, T. Song, J. Gao, and S. Shi, Cluster expansion method and its application in computational materials science, Comput. Mater. Sci. **125**, 243 (2016).

[68] G. Kresse and J. Furthmüller, Efficient iterative schemes for *ab initio* total-energy calculations using a plane-wave basis set, Phys. Rev. B **54**, 11169 (1996).

[69] J. P. Perdew, K. Burke, and M. Ernzerhof, Generalized Gradient Approximation Made Simple, Phys. Rev. Lett. **77**, 3865 (1996).

[70] See Supplemental Material at http://link.aps.org/supplemental/10.1103/PhysRevB.106.024114 for more detailed structures, lattice parameters, and mechanical properties for monolayer $Si_{1-x}Ge_x$.

[71] G. Hart and R. Forcade, Algorithm for generating derivative structures, Phys. Rev. B **77**, 224115 (2008).

[72] O. Aktas, S. Z. Oo, S. J. MacFarquhar, V. Mittal, H. M. H. Chong, and A. C. Peacock, Laser-driven phase segregation and tailoring of compositionally graded microstructures in Si–Ge nanoscale thin films, ACS Appl. Mater. Interfaces **12**, 9457 (2020).

[73] V. O. Özçelik, N. Garg, and C. E. White, Symmetry-induced stability in alkali-doped calcium silicate hydrate, J. Phys. Chem. C **123**, 14081 (2019).

[74] X. Ma, T. Yang, D. Li, and Y. Feng, Phase stability of monolayer $Si_{1-x}Ge_x$ alloys with a dirac cone, Nanoscale **13**, 8607 (2021).

[75] F. Mouhat and F.-X. Coudert, Necessary and sufficient elastic stability conditions in various crystal systems, Phys. Rev. B **90**, 224104 (2014).

[76] G. Grimvall, B. Magyari-Köpe, V. Ozoliņš, and K. A. Persson, Lattice instabilities in metallic elements, Rev. Mod. Phys. **84**, 945 (2012).

[77] B. Mortazavi, O. Rahaman, M. Makaremi, A. Dianat, G. Cuniberti, and T. Rabczuk, First-principles investigation of mechanical properties of silicene, germanene and stanene, Physica E: Low Dimens. Syst. Nanostruct. **87**, 228 (2017).

[78] L. Shi, J. Jiang, G. Zhang, and B. Li, High thermoelectric figure of merit in silicon-germanium superlattice structured nanowires, Appl. Phys. Lett. **101**, 233114 (2012).

[79] X. Wang, Y. Hong, P. K. L. Chan, and J. Zhang, Phonon thermal transport in silicene-germanene superlattice: A molecular dynamics study, Nanotechnology **28**, 255403 (2017).

[80] Y. Chalopin, K. Esfarjani, A. Henry, S. Volz, and G. Chen, Thermal interface conductance in Si/Ge superlattices by equilibrium molecular dynamics, Phys. Rev. B **85**, 195302 (2012).

[81] X. Qin, Y. Liu, X. Li, J. Xu, B. Chi, D. Zhai, and X. Zhao, Origin of Dirac cones in SiC silagraphene: A combined density functional and tight-binding study, J. Phys. Chem. Lett. **6**, 1333 (2015).